

Fe₃O₄@astragalus polysaccharide core-shell nanoparticles for iron deficiency anemia therapy and magnetic resonance imaging *in vivo*

Kai Wang, Lina Li, Xiaoguang Xu, Liying Lu, Jian Wang, Shuyan Wang, Yining Wang, Zhengyu Jin, Jin Zhong Zhang, Yong Jiang **

K. Wang, Prof. X. G. Xu, Prof. Y. Jiang. Beijing Advanced Innovation Center for Materials Genome Engineering, School of Materials Science and Engineering,

University of Science and Technology Beijing, Beijing 100083, China

E-mail: xgxu@ustb.edu.cn (X.G. Xu), yjiang@ustb.edu.cn (Y. Jiang)

Prof. L. N. Li, S. Y. Wang. School of Chinese Medicine, Beijing University of Chinese Medicine, Beijing 100029, China

Prof. L.Y. Lu. School of Chemistry and Biological Engineering, University of Science and Technology Beijing, Beijing 100083, China

Dr. J. Wang, Prof. Y. N. Wang, Prof. Z. Y. Jin. Department of Radiology, Peking Union Medical College Hospital, Chinese Academy of Medical Sciences, Beijing 100730, China

Prof. J. Z. Zhang. Department of Chemistry & Biochemistry, University of California, Santa Cruz, CA 95064, USA

ABSTRACT: Fe_3O_4 @astragalus polysaccharide core-shell nanoparticles (Fe_3O_4 @APS NPs) were demonstrated to be an efficient therapeutic drug for treating iron deficiency anemia (IDA) *in vivo*. The Fe_3O_4 @APS NPs have been synthesized using a two steps approach involving hydrothermal synthesis and subsequent esterification. Transmission electron microscopy (TEM) and Fourier transform infrared (FTIR) spectroscopy studies show that APS are attached on the surfaces of the highly monodisperse Fe_3O_4 NPs. Dynamic light scattering (DLS) and magnetic characterizations reveal that the Fe_3O_4 @APS NPs have outstanding water solubility and stability. Cytotoxicity assessment using Hela cells and pathological tests in mice demonstrate their good biocompatibility and low toxicity. The IDA treatment in rats shows that they have efficient therapeutic effect, which is contributed to both the iron element supplement from Fe_3O_4 and the APS-stimulated hematopoietic cell generation. Moreover, the Fe_3O_4 @APS NPs are superparamagnetic and thus able to be used for magnetic resonance imaging (MRI). This study has demonstrated the potential of nanocomposites involving purified natural products from Chinese herb medicine for biomedical applications.

Iron is one of the most important trace elements in human body and is essential for the normal function of organisms, particularly for the metabolism and immune functions. ^[1] As reported by World Health Organization, 2 billion people have anemia, with nearly 1 billion suffering from iron deficiency anemia (IDA).^[2] Therefore, IDA is a common nutritional disease in modern society.^[3] Oral iron supplementation, such as ferrous salts, is common in the treatment and prevention of iron deficiency in human body.^[4] However, it usually causes side effects, such as epigastric pain, diarrhea and constipation.^[5] Therefore, it is highly desired to develop new iron supplements with no or few side effects.^[6]

Ferumoxide, known as Feridex in America and Endorem in Europe, is a colloid of ultra-small superparamagnetic iron oxide (USPIO) nanoparticles (NPs) coated by dextran.^[7] It is a FDA-cleared drug for the treatment of IDA in adult chronic kidney disease patients. ^[8] ^[9] After intravenous administration, the USPIO NPs are cleared from blood by phagocytosis.^[10] The USPIO NPs are metabolized in the lysosomes into a soluble, nonmagnetic form of iron that becomes part of the normal iron pool after the intracellular uptake. Among the USPIO NPs, Fe₃O₄ NPs have been proved to exhibit good superparamagnetic property below 15 nm and can be used as both an iron supplement and a magnetic resonance imaging (MRI) contrast agent candidate.
^[11]

MRI is a powerful noninvasive diagnostic technique for visualizing the fine structure of the human body with high spatial resolution. To obtain accurate diagnosis, contrast agents are usually used to increase the MRI image quality by exerting an

influence on the longitudinal (T_1), transverse (T_2) relaxation time and T_2 -star (T_2^*), a relaxation parameter arising principally from local magnetic field in homogeneities that are increased with iron deposition.^[12] Due to the unique superparamagnetic property, Fe_3O_4 NPs have been widely used as ultrasensitive negative contrast agents for early detection of tumors due to their strong T_2 and T_2^* shortening effect.^[13]

Unfortunately, the exposed Fe_3O_4 NPs have poor solubility and biocompatibility. Therefore, the surface of Fe_3O_4 NPs needs to be suitably engineered to acquire improved biocompatibility.^[14, 15] The most popular methods are introducing hydrophilic groups and modification of bioinorganic shell on the surface of Fe_3O_4 NPs, which can effectively optimize the properties of Fe_3O_4 NPs to satisfy the requirements of applications, such as MRI contrast agents,^[16] magnetic targeting drug, biomolecule separation, and hyperthermal cancer therapy.^[17] For example, Fe_3O_4 -based nanocomposites, such as Fe_3O_4 @Polydopamine,^[18] WS_2 @ Fe_3O_4 ,^[19] Fe_3O_4 @Au^[20] and C- Fe_3O_4 quantum dots (QDs)^[21], have been studied as MRI contrast agents and drug carriers in preclinical and clinical setting.^[22]

Among the modification materials of Fe_3O_4 NPs, polysaccharides have the advantages of stability, water solubility and few side effects on the organism. Meanwhile, some natural polysaccharides can promote the formation of hematopoietic cell.^[23] *Astragalus membranaceus*, a traditional Chinese herb medicine containing many active components, such as polysaccharides, flavonoids, saponins, amino acids and trace elements, has been used in China for medicine for more than 2,000 years to improve human immunity and treat cardiovascular disorders.

Astragalus polysaccharide (APS) is one of the main active components of Astragalus membranaceus extracted from Astragalus roots, which is described in the 2005 version of the “Chinese Pharmacopoeia”.^[24] APS is comprised of uniform polysaccharide fraction, including rhamnose, arabinose and glucose.^[25] APS is stable and biocompatible *in vivo*, which makes it an ideal material for biomedical applications. Many reports on the biological activities of APS indicate that it possesses potent anti-inflammatory, organ protective, anti-tumor activities and growth of red blood cell stimulative.^[26] Therefore, APS is a promising material for modifying Fe₃O₄ NPs.

To develop a potential IDA therapeutic agent combining iron supplements and contents of promoting the hematopoietic cell formation, we report a novel material of Fe₃O₄@APS Core-Shell NPs fabricated by a two steps approach involving hydrothermal synthesis^[27] and esterification. As shown in **Figure 1a**, the water soluble Fe₃O₄ NP cores were obtained in sodium citrate solution, in which sodium citrate replaces the oleic acid molecular on the surface of the Fe₃O₄ NPs. Then, The Fe₃O₄ NPs were bonded with the APS backbone, and the sodium citrate reacted with the hydroxyl groups of the APS chains to form the Fe₃O₄@APS NPs. Finally, the Fe₃O₄@APS NPs were used in mice intragastric administration for IDA treatment and MRI testing followed by pathological tests, after the structural stability characterization and cytotoxicity assessment, as depicted in **Scheme 1**. As expected, the Fe₃O₄@APS NPs show unique therapeutic effect for IDA treatment, which is much better than that of water soluble Fe₃O₄ NPs. This is the result of the combined

contribution of the hematopoietic cell generation stimulated by APS and the simultaneous iron element supplement from Fe₃O₄. Besides this, the Fe₃O₄@APS NPs are also potential MRI contrast agents *in vivo*, which are safe and good for health. The study opens a new way to design IDA medicine with USPIO NPs and natural polysaccharides, which can serve as a contrast agent at the same time.

The crystal structural of the Fe₃O₄ NPs and Fe₃O₄@APS NPs were investigated by X-ray diffraction (XRD) (Figure S2, Supporting Information). The XRD patterns of both NP samples show sharp diffraction peaks of Fe₃O₄ (JCPDS75-0033)^[28] with Fd-3m space group, indicating good crystallinity. Figure 1b shows the transmission electron microscope (TEM) image of the oil-soluble Fe₃O₄ NPs, which are spherical with a uniform diameter of ~10 nm. High-resolution TEM images of the Fe₃O₄ NPs exhibit (220) and (331) crystal facets as indexed in Figure 1c. The hydrodynamic diameter of the water soluble Fe₃O₄ NPs was measured to be 11 nm by dynamic light scattering (DLS) (Figure 1e), which is slightly larger than that measured by TEM (Figure 1d).

For the Fe₃O₄@APS NPs, the diameter does not show obvious increase in TEM image (Figure 1f), revealing clear cores of Fe₃O₄ NPs but insignificant evidence of the APS shells. This is because APS molecules are composed by C, H, O and N elements, which are invisible in TEM. However, the DLS results show a mean size of 29.5 nm for the Fe₃O₄@APS NPs (Figure 1g), which demonstrates the existence of the APS shells coated on the surface of Fe₃O₄ NPs. The dispersion stability of the oleic acid-coated Fe₃O₄ NPs shows good water stability and biocompatibility after the

ligand exchange reaction on the surface from oleic acid to sodium citrate and APS. The zeta potential of the water soluble Fe₃O₄ NPs and Fe₃O₄@APS NPs are -36.8 mV and -28.8 mV, respectively, which suggests good water dispersity of the NPs (Figure S3, Supporting Information).^[29]

Fourier transform infrared (FT-IR) absorption spectra were measured to confirm the presence of the APS around the Fe₃O₄ NPs (Figure 1h). Compared to the FT-IR spectrum of Fe₃O₄ around with oleic acid, the one of Fe₃O₄@APS NPs shows new strong absorption bands at 1383 cm⁻¹ and 1633 cm⁻¹, which can be attributed to the C-O-C and C=O stretch of APS and sodium citrate vibration of polysaccharide, respectively. It is evident that the oleic acid on the surface of Fe₃O₄ NPs was efficiently replaced by APS and sodium citrate. Moreover, the Fe₃O₄@APS NPs show a strong absorption band at 586 cm⁻¹, attributed to Fe-O bond, while the APS copolymer has the stretching bands at 2921 cm⁻¹ and 3424 cm⁻¹, corresponding to hydroxyl groups, which are a further evidence of the ligand exchange on the surface of Fe₃O₄ NPs.

To study the magnetic properties of Fe₃O₄@APS NPs, the magnetization curves have been measured, as shown in Figure 1i. All the curves exhibit no hysteresis, suggesting that the Fe₃O₄ NPs are superparamagnetic, with or without APS coating. The Fe₃O₄ NPs have a higher saturation magnetization (M_s) (about 62.2 emu/g) than that of the Fe₃O₄@APS NPs (about 36.7 emu/g), which further demonstrates the existence of the APS shells on the surface of Fe₃O₄ NPs. From the change of M_s , the mass percentage of the Fe₃O₄ NPs can be estimated to be around 60% in the

Fe_3O_4 @APS NPs. With a magnet placed outside the cuvette, the Fe_3O_4 @APS NPs in the water solution can rapidly accumulate near the magnet (See the inset of Figure 1i). When the magnet is removed, the Fe_3O_4 @APS NPs disperse in water again, even after 6 months, suggesting the Fe_3O_4 @APS NPs are superparamagnetic with good stability. To further investigate the magnetic behavior of the Fe_3O_4 @APS NPs, the temperature dependence of their magnetization was investigated by zero-field cooling (ZFC) and field cooling (FC) respectively (Figure S4, Supporting Information). The $M_{\text{ZFC}}-T$ curves show broad peaks with a clear maximum (T_{max}) at ~ 226 K for the Fe_3O_4 NPs and ~ 167 K for the Fe_3O_4 @APS NPs, above which temperature the particles are in superparamagnetic regime. Thus, both kinds of the NPs are superparamagnetic at 300 K.^[14]

Since the Fe_3O_4 @APS NPs should be fed to the Institute of Cancer Research (ICR) mice and Wistar rats, it is possible that the Fe_3O_4 @APS NPs might be degraded during digestion in their stomachs. Thus, we have checked the stability of the Fe_3O_4 @APS NPs in imitated gastric acid by stirring in HCl solution with pH = 1.5 for 5 h. The magnetization curve of the Fe_3O_4 @APS NPs collected after the imitating digestion still shows good superparamagnetic property (as shown in Figure 1i). The M_s of the Fe_3O_4 @APS NPs increases to 45.6 emu/g, which is larger than that of the as-prepared Fe_3O_4 @APS NPs. This suggests that a certain amount of APS molecules could desorb from the NPs surfaces in the stomach due to the acid environment. However, comparing with the M_s of the Fe_3O_4 NPs, we confirmed that there is still sufficient amount of APS molecules attached to the Fe_3O_4 NPs cores. Moreover, the

FT-IR spectrum of the Fe₃O₄@APS NPs (Figure 1h) shows no significant change relative to that of the as-prepared Fe₃O₄@APS NPs, consistent with the results of the magnetic studies. The iron concentration in the Fe₃O₄@APS NPs was also quantitatively determined by inductively coupled plasma optical emission spectroscopy (ICP-OES). The weight percentage of Fe increases from 60% to 75% after stirring in HCl solution, which is consistent with the change of the magnetization curves. Accordingly, only a small amount of APS molecules were degraded by HCl solution. Therefore, the Fe₃O₄@APS NPs are stable enough and can be absorbed into blood as whole NPs, instead of the separate Fe₃O₄ NPs and APS.

The cytotoxicity evaluation is necessary for a new biomaterial before *in vivo* applications. We assessed the biocompatibility of the Fe₃O₄@APS NPs with mammalian cells by a 3-(4,5-dimethylthiazol-2-yl)-2,5-diphenyltetrazolium bromide (MTT) assay using a HeLa cell line. As shown in **Figure 2a**, the cell viabilities are higher than 75% after 24 h, 48 h and 72 h exposure to the iron concentration of 0-50 $\mu\text{g/mL}$. There is no decrease in cell viability when the exposure time was prolonged to 72 h. Therefore, the Fe₃O₄@APS NPs have a high biocompatibility and low cytotoxicity.

The MRI performance of the Fe₃O₄@APS NPs as contrast agents has been studied both *in vitro* and *in vivo*. For comparison, the Fe₃O₄ NPs have also been investigated. Figure 2b shows the T_2^* MRI images of the Fe₃O₄ NPs and Fe₃O₄@APS NPs suspensions at different Fe concentrations. The low signal intensities in the T_2^* MRI images increase with Fe concentration for both kinds of nanoparticles. Moreover, the

intensities are similar when the Fe concentration in the Fe₃O₄ NPs and Fe₃O₄@APS NPs suspensions are approximately equal. As a negative MRI contrast agent, the superparamagnetic Fe₃O₄ core can shorten the T_2^* values of water, resulting in a hyperintense signal on T_2^* imaging. In addition, the T_2^* relaxation rate ($r_2^* = 1/T_2^*$) of the Fe₃O₄ NPs and Fe₃O₄@APS NPs was calculated to be 483 mM⁻¹s⁻¹ (Figure 2c) and 400 mM⁻¹s⁻¹ (Figure 2d), respectively. The observed decrease in the r_2^* value can be attributed to the APS on the surface of Fe₃O₄ NPs, which weakens the magnetic properties of the NPs. However, the Fe₃O₄@APS NPs remain a good contrast agent for MRI applications.

The preliminary *in vitro* MRI signal contrast enhancement of the Fe₃O₄@APS NPs led us to evaluate its possibility to serve as a negative MRI contrast agent for MRI *in vivo* imaging. Fe₃O₄@APS NPs were gastrically infused into the stomach of live healthy male ICR mice at a dosage of 10 mg/kg. Figure 2e shows the T_1 and T_2 weighted MRI images of the reference group (normal mice) and the mice after gastric infusion for 15 min. Comparing to the reference group, the T_1 and T_2 images for the mice after the gastric infusion show a positive and a negative contrast enhancement in the stomach and the bowels, respectively. Therefore, the Fe₃O₄@APS NPs have a significant signal enhancement effect as a MRI contract agent. The MRI images of the main organs have no specific changes even after being perfused for 4 h, 8 h and 16 h (Figure S5, Supporting Information), indicating the safety during Fe₃O₄@APS NPs metabolism.

In vivo toxicity and possible side effects of nanomedicines have to be carefully

studied before practical applications in clinic. In order to further demonstrate the safety of the Fe₃O₄@APS NPs, the stomachs of healthy male ICR mice were perfused with the Fe₃O₄@APS NPs at a dosage of 1.0 mg/kg/d and 2.0 mg/kg/d, respectively. On the 15th and 30th day, the mice were tested by MRI to examine the effect of the Fe₃O₄@APS NPs on the organs such as liver and kidney. **Figure 3a** and Figure S6a (Supporting Information) show the T_2 -weighted images of the livers and kidneys of the mouse treated by 1.0 mg/kg/d and 2.0 mg/kg/d of Fe₃O₄@APS NPs on the 30th and 15th day, together with that of the normal mouse as contrast group. Comparing with the contrast group, there is no obvious damage in the groups treated by Fe₃O₄@APS NPs. The T_2^* values shown in Figure 3b and Figure S6b (Supporting Information) also reveal no particular change in T_2^* values of the kidney and the liver in the range of the organ regions with different dosage and time. These results demonstrate that no pathological change happened in the organs of the ICR mice after a long time supplementation of the Fe₃O₄@APS NPs.

The histopathological studies were carried out on the main organs of the ICR mice after the *in vivo* MRI testing. The histopathological images of the livers, kidneys and brains are presented in Figure 3c and Figure S7 (Supporting Information), which correspond to the ICR mice after the intragastric administration of Fe₃O₄@APS NPs for 30 and 15 days, respectively. As expected, no particles were observed in the organs, and no sign of organ damage or inflammation was observed, demonstrating the minimal side effects of the Fe₃O₄@APS NPs *in vivo* after 30 days intragastric administration.

To study the effect of the Fe₃O₄@APS NPs on IDA, low-iron diet Wistar rats were separated into different groups and fed with the designed ferralia dosage. The rats were weighted every week. As shown in Figure 3d, the mean body weights of all groups increase almost linearly with time. As expected, the model group shows the smallest slope of the weight growth due to serious IDA. The group treated with the Fe₃O₄ NPs has a weight growth rate higher than the model group but lower than the other treated and normal groups without IDA. However, the groups treated with the Fe₃O₄@APS NPs have weight growth rates comparable to that of the normal group, and a higher Fe₃O₄@APS NPs dosage results in a larger weight growth rate. Therefore, the Fe₃O₄@APS NPs treatment can improve the health of the low-iron diet rats.

The Hemoglobin (HGB), Hemoglobin (RBC) and Hematocrit (HCT) are important parameters for the diagnosis and therapy of IDA. Therefore, the blood analyses were carried out for the rats studied, and the results are presented in Figure 3e-3g. Usually, the rats are considered as anemic when the HGB level is reduced to 75% of the original level. As shown in Figure 3e, the HGB values of the low-iron diet groups are only half of that of the normal group before ferralia treatment, which indicates a serious IDA of the low-iron diet rats. After the ferralia treatment, all the treated groups have significant increase of HGB values, while only the group supplied with the Fe₃O₄@APS NPs at a dosage of 2.0 mg/kg/d has a HGB value (136 g/L) comparable to the normal group (143.1 g/L). The group treated with the 1.0 mg/kg/d Fe₃O₄@APS NPs (117.1 g/L) has a curative effect similar to the group of the 2.0 mg/kg/d Fe₃O₄

NPs (117.2 g/L), demonstrating that the Fe₃O₄@APS NPs have more positive effect on HGB than the Fe₃O₄ NPs. The other two important parameters, RBC and HCT, have the trends similar to that of HGB. All blood analyses suggest that the health condition of the group supplied by the 2.0 mg/kg/d Fe₃O₄@APS NPs recovered to the level of the normal group. Moreover, the superoxide dismutase (SOD), glutathione (GSH), lactic dehydrogenase (LDH), hepcidin (HEP), malondialdehyde (MDA) and serum iron (SI) data were also measured after 30 days of the treatment. All results (Table S1, Supporting Information) demonstrate the high therapeutic effect of the Fe₃O₄@APS NPs on IDA *in vivo*. Considering the structure of the Fe₃O₄@APS NPs, their high therapeutic effect is attributed to both iron element supplement from Fe₃O₄ and the APS stimulated hematopoietic cell generation. As a result, the Fe₃O₄@APS NPs are highly promising as an IDA drug with the additional benefit of serving as a MRI contrast agent.

In conclusion, we have designed and experimentally demonstrated the Fe₃O₄@APS NPs for the targeting IDA treatment and the MRI contract agent. The stability of the Fe₃O₄@APS NPs was determined by the imitating digestion in imitated gastric acid. Both *in vitro* and *in vivo* toxicity studies were carried out using the cell experiments and intragastric administration of animal model. The blood analyses show that the Fe₃O₄@APS NPs have potent therapeutic effect on IDA, evidenced by the HGB, RBC and HCT values of the 2.0 mg/kg/d Fe₃O₄@APS NPs treated IDA rats. Moreover, strong MRI contrast enhancement has been observed for the Fe₃O₄@APS NPs. Therefore, the Fe₃O₄@APS NPs are promising candidates for IDA drugs with the

additional functionality as MRI contract agent.

Supporting Information

Supporting Information is available from the Wiley Online Library or from the author.

Acknowledgements

K. Wang and L. N. Li contributed equally to this work. This work was partially supported by the National Basic Research Program of China (Grant No. 2015CB921502), the National Science Foundation of China (Grant Nos. 51671019, 51471029, 51731003, 61471036) and Beijing science and technology Nova cross program (Z171100001117136).

Conflict of Interest

The authors declare no conflict of interest.

Keywords

Fe₃O₄ nanoparticles, astragalus polysaccharides, iron deficiency anemia, magnetic resonance imaging.

References

- [1] S. Denic, M. M. Agarwal, *Nutrition* **2007**, *23*, 603.
- [2] T. Vos, C. Allen, M. Arora, R. M. Barber, Z. A. Bhutta, A. Brown, ... & C. J. L. Murray, *Lancet* **2016**, *388*, 1545.
- [3] A. Lopez, P. Cacoub, I. C. Macdougall, L. Peyrin-Biroulet, *Lancet* **2016**, *387*, 907.
- [4] C. Camaschella, *N. Engl. J. Med.* **2015**, *372*, 1832.
- [5] G. D. Lewis, R. Malhotra, A. F. Hernandez, S. E. McNulty, A. Smith, G. M. Felker, W. H. W. Tang, S. J. LaRue, M. M. Redfield, M. J. Semigran, M. M. Givertz, P. Van Buren, D. Whellan, K. J. Anstrom, M. R. Shah, P. Desvigne-Nickens, J. Butler, E. Braunwald, *JAMA* **2017**, *317*, 1958.
- [6] S. D. Anker, G. Filippatos, R. Willenheimer, K. Dickstein, H. Drexler, ... & P. Ponikowski, *N. Engl. J. Med.* **2009**, *361*, 2436.
- [7] P. R. Ros, P. C. Freeny, S. E. Harms, S. E. Seltzer, P. L. Davis, T. W. Chan, A. E. Stillman, L. R. Muroff, V. M. Runge, M. A. Nissenbaum, *Radiology* **1995**, *196*, 481.
- [8] D. W. Coyne, *Expert Opin. Pharmacother.* **2009**, *10*, 2563.
- [9] J. T. Ferrucci, D. D. Stark, *AJR, Am. J. Roentgenol.* **1990**, *155*, 943.
- [10] A. Khurana, H. Nejadnik, F. Chapelin, O. Lenkov, R. Gawande, S. Lee, S. N. Gupta, N. Aflakian, N. Derugin, S. Messing, G. Lin, T. F. Lue, L. Pisani, H. E. Daldrup-Link, *Nanomedicine* **2013**, *8*, 1969.
- [11] a) S. Zanganeh, G. Hutter, R. Spitler, O. Lenkov, M. Mahmoudi, A. Shaw, J. S. Pajarinen, H. Nejadnik, S. Goodman, M. Moseley, L. M. Coussens, H. E.

- Daldrup-Link, *Nat. Nanotechnol.* **2016**, *11*, 986; b) Z. Gao, Y. Hou, J. Zeng, L. Chen, C. Liu, W. Yang, M. Gao, *Adv. Mater.* **2017**, *29*, 1701095.
- [12]a) Y. X. J. Wang, S. M. Hussain, G. P. Krestin, *Eur. Radiol.* **2001**, *11*, 2319; b) Y. Wang, K. Zhou, G. Huang, C. Hensley, X. Huang, X. Ma, T. Zhao, B. D. Sumer, R. J. DeBerardinis, J. Gao, *Nat. Mater.* **2014**, *13*, 204.
- [13]R. Hao, R. Xing, Z. Xu, Y. Hou, S. Gao, S. Sun, *Adv. Mater.* **2010**, *22*, 2729.
- [14]C. Scialabba, R. Puleio, D. Peddis, G. Varvaro, P. Calandra, G. Cassata, L. Cicero, M. Licciardi, G. Giammona, *Nano Res.* **2017**, *10*, 3212.
- [15]J. Zeng, L. Jing, Y. Hou, M. Jiao, R. Qiao, Q. Jia, C. Liu, F. Fang, H. Lei, M. Gao, *Adv. Mater.* **2014**, *26*, 2694.
- [16]J. Yu, C. Yang, J. Li, Y. Ding, L. Zhang, M. Z. Yousaf, J. Lin, R. Pang, L. Wei, L. Xu, F. Sheng, C. Li, G. Li, L. Zhao, Y. Hou, *Adv. Mater.* **2014**, *26*, 4114.
- [17]S. Tong, C. A. Quinto, L. Zhang, P. Mohindra, G. Bao, *ACS nano* **2017**, *11*, 6808.
- [18]L. S. Lin, Z. X. Cong, J. B. Cao, K. M. Ke, Q. L. Peng, J. Gao, H. H. Yang, G. Liu, X. Chen, *ACS nano* **2014**, *8*, 3876.
- [19]G. Yang, H. Gong, T. Liu, X. Sun, L. Cheng, Z. Liu, *Biomaterials* **2015**, *60*, 62.
- [20]a) C. Li, T. Chen, I. Ocsoy, G. Zhu, E. Yasun, M. You, C. Wu, J. Zheng, E. Song, C. Z. Huang, W. Tan, *Adv. Funct. Mater.* **2014**, *24*, 1772; b) W. Dong, Y. Li, D. Niu, Z. Ma, J. Gu, Y. Chen, W. Zhao, X. Liu, C. Liu, J. Shi, *Adv. Mater.* **2011**, *23*, 5392; c) L. S. Lin, X. Yang, Z. Zhou, Z. Yang, O. Jacobson, Y. Liu, A. Yang, G. Niu, J. Song, H. H. Yang, X. Chen, *Adv. Mater.* **2017**, *29*, 1606681.

- [21] X. Liu, H. Jiang, J. Ye, C. Zhao, S. Gao, C. Wu, C. Li, J. Li, X. Wang, *Adv. Funct. Mater.* **2016**, *26*, 8694.
- [22] a) Z. Wang, R. Qiao, N. Tang, Z. Lu, H. Wang, Z. Zhang, X. Xue, Z. Huang, S. Zhang, G. Zhang, Y. Li, *Biomaterials* **2017**, *127*, 25. b) X. Wang, D. Niu, P. Li, Q. Wu, X. Bo, B. Liu, S. Bao, T. Su, H. Xu, Q. Wang, *ACS nano* **2015**, *9*, 5646.
- [23] a) Z. Liu, Y. Jiao, Y. Wang, C. Zhou, Z. Zhang, *Adv. Drug Deliv. Rev.* **2008**, *60*, 1650; b) M. Swierczewska, H. S. Han, K. Kim, J. H. Park, S. Lee, *Adv. Drug Delivery Rev.* **2016**, *99*, 70.
- [24] a) B. M. Shao, W. Xu, H. Dai, P. Tu, Z. Li, X. M. Gao, *Biochem. Biophys. Res. Commun.* **2004**, *320*, 1103; b) X. Q. Ma, Q. Shi, J. A. Duan, T. T. X. Dong, K. W. K. Tsim, *J. Agric. Food Chem.* **2002**, *50*, 4861.
- [25] J. H. Xie, M. L. Jin, G. A. Morris, X. Q. Zha, H. Q. Chen, Y. Yi, J. E. Li, Z. J. Wang, J. Gao, S. P. Nie, P. Shang, M. Y. Xie, *Crit. Rev. Food Sci. Nutr.* **2016**, *56*, S60.
- [26] Q. Lu, L. Xu, Y. Meng, Y. Liu, P. Li, Y. Zu, M. Zhu, *Int. J. Biol. Macromol.* **2016**, *93*, 208.
- [27] S. Si, C. Li, X. Wang, D. Yu, Q. Peng, Y. Li, *Cryst. Growth Des.* **2005**, *5*, 391.
- [28] M. E. Fleet, *Acta Crystallogr., Sect. C: Cryst. Struct. Commun.* **1984**, *40*, 1491.
- [29] S. Bhattacharjee, *J. Controlled Release* **2016**, *235*, 337.

Figure Captions

Scheme 1. Schematic illustration of the design and application of Fe₃O₄@APS NPs for IDA therapy and MRI.

Figure 1. a) Schematic drawing the synthesis of the Fe₃O₄@APS NPs. b) TEM and c) high-resolution TEM images of the oil soluble Fe₃O₄ NPs. d) TEM image of water soluble Fe₃O₄ NPs and e) their hydrodynamic profiles. f) TEM image of Fe₃O₄@APS NPs and g) their hydrodynamic profiles. h) FT-IR spectra and i) magnetization curves of the Fe₃O₄ NPs, Fe₃O₄@APS NPS and Fe₃O₄@APS NPs after stirring in HCl solution. Inset of i) is the image of the Fe₃O₄@APS NPs in water dispersion with (right) and without (left) external field.

Figure 2. a) Cell viability of Hela cells after treatment with the Fe₃O₄@APS NPs at different iron concentrations after 24h, 48h and 72h. b) T_2^* images of the Fe₃O₄ NPs and Fe₃O₄@APS NPs water solution with different Fe concentrations. Corresponding T_2^* relaxation rate of the Fe₃O₄ NPS c) and the Fe₃O₄@APS NPs d) with respect to iron concentration. e) T_1 -weighted and T_2 -weighted MRI images of contrast group (normal mouse) and the Fe₃O₄@APS NPs gastric infused Male ICR mouse after 15 min.

Figure 3. a) *In vivo* T_2 -weighted images of the male ICR mice liver and kidney for

contract group and the group treated with the Fe₃O₄@APS NPs at different Fe concentrations after 30 days. b) Signal intensity of T₂* values of liver and kidney. c) H&E stained organ slices of the mice after 30 days Fe₃O₄@APS NPs treatment. Scale bars for all images are 100 μm. d) Body Weight increase with time, e) HGB concentration, f) RBC concentration and g) HCT values of male Wistar rats (8 per group) before and after 30 days treatment with the Fe₃O₄@APS NPs intragastric administration.

Scheme 1. (Wang K. et al.)

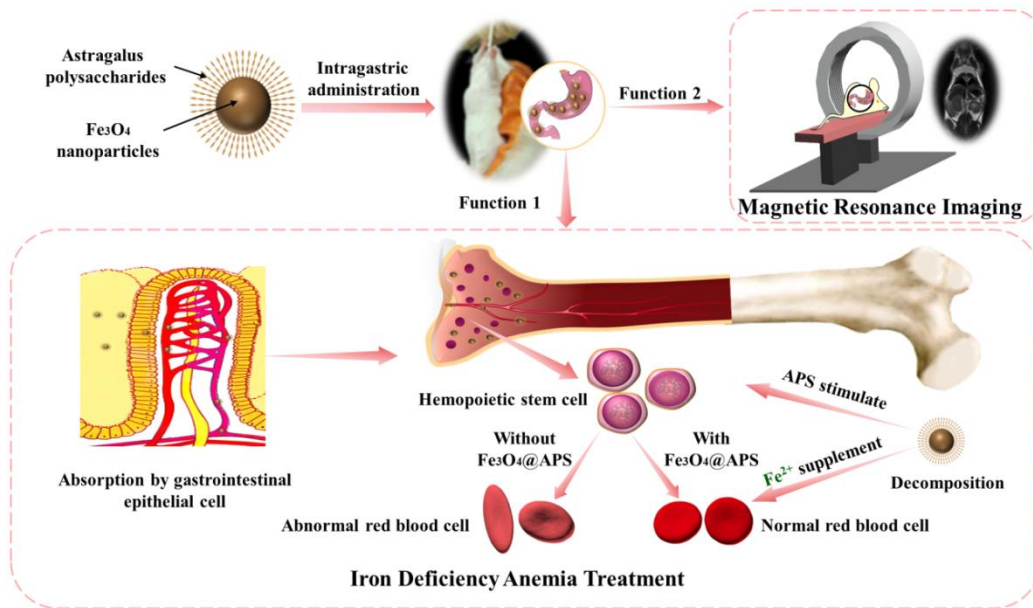


Figure 1. (Wang K. et al.)

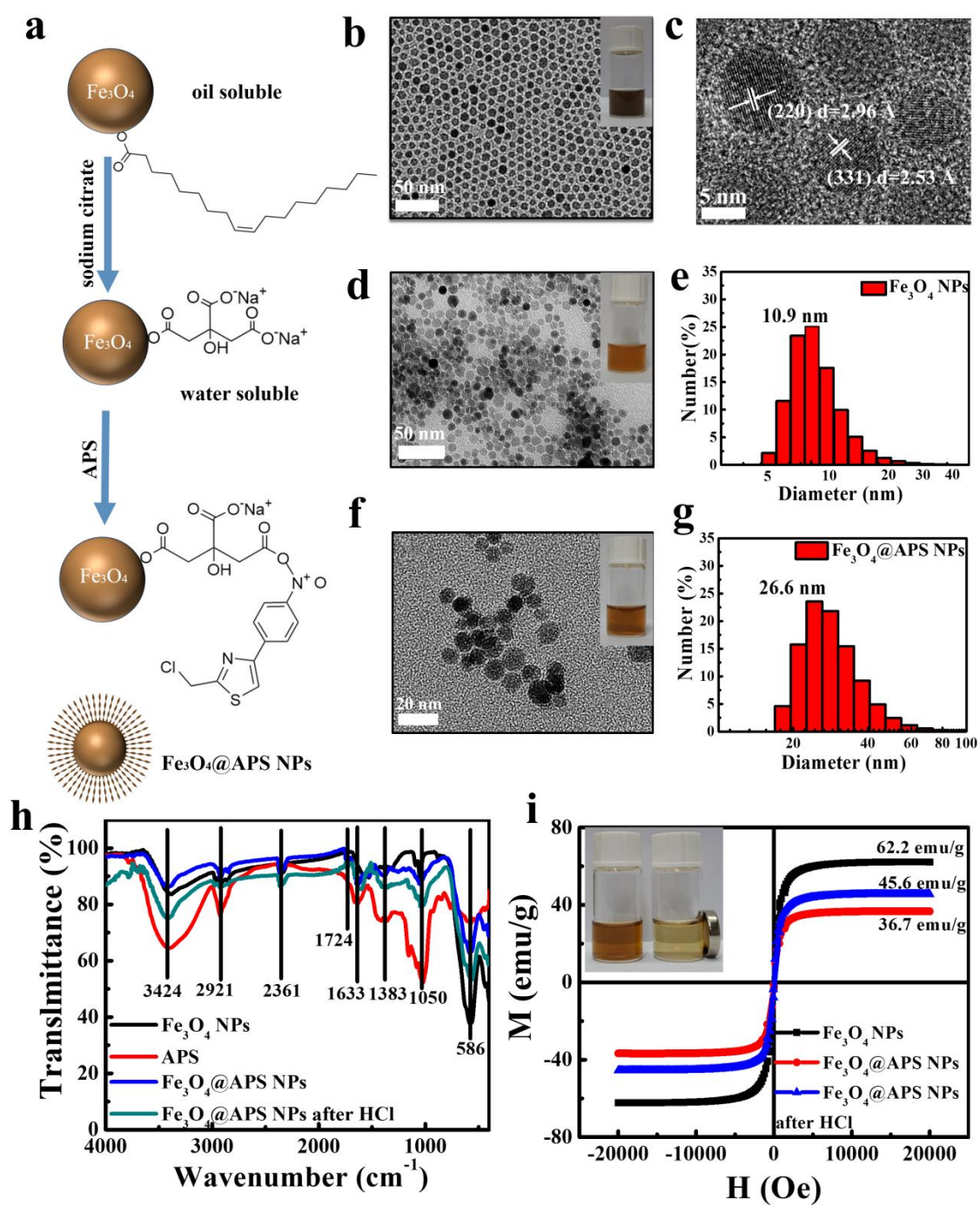


Figure 2. (Wang K. et al.)

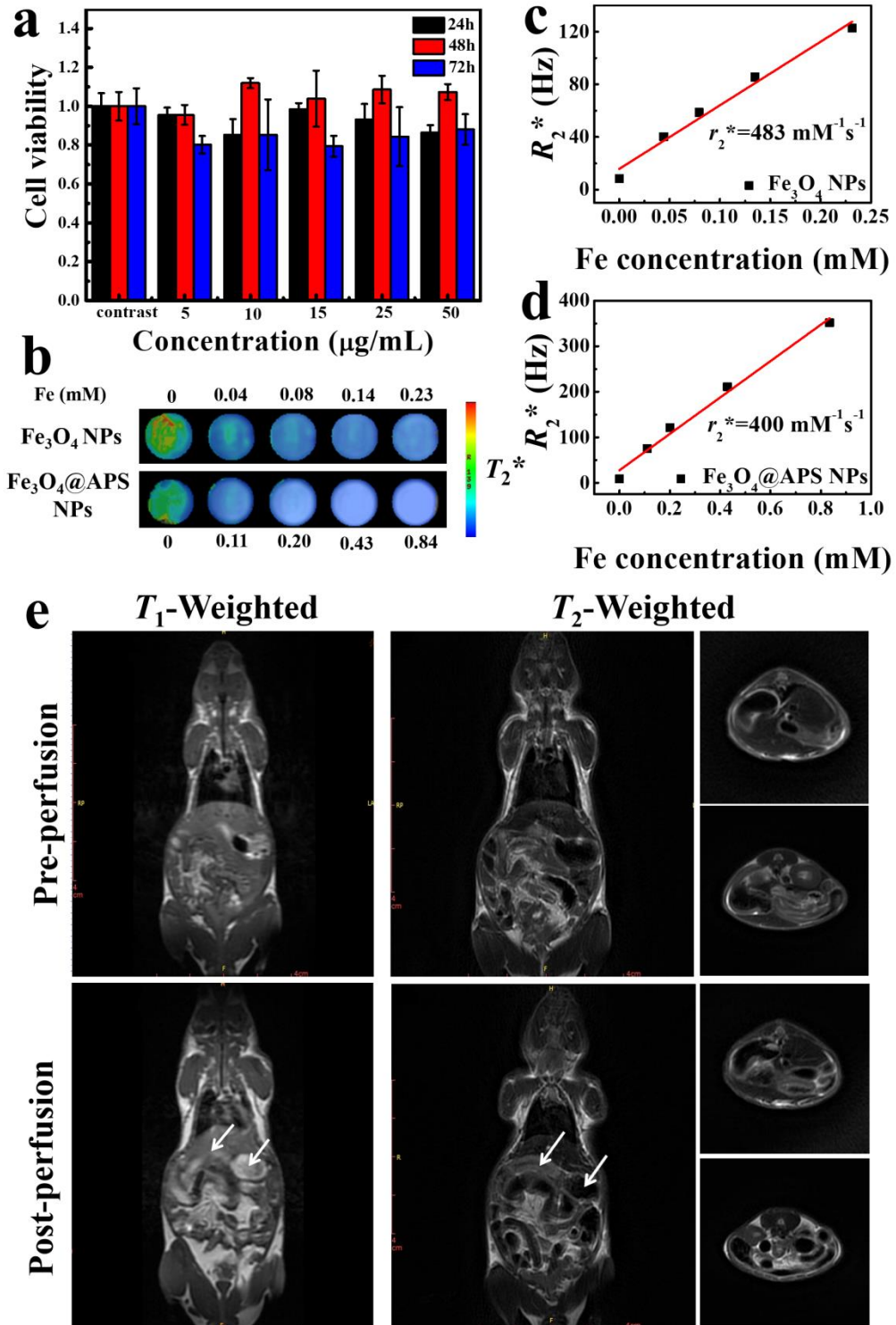


Figure 3. (Wang K. et al.)

